Passband Control of Lightly Damped Systems With Mode Separation

Timothy N. Chang, *Member, IEEE*, and Nirwan Ansari, *Senior Member, IEEE*

***Abstract*—This paper deals with the regulation and stabilization of lightly damped systems under plant uncertainty. A controller consisting of a neural-network-based mode separator together with a modular passband tuning regulator is proposed. The mode separator generates the in-phase components of the plant utilized by the passband tuning regulator to maintain closed-loop stability and asymptotic regulation. This combined controller is robust and requires minimal plant information to operate. A synthesis procedure is outlined in this paper to summarize the design steps in a systematic manner. Finally, the application of the passband controller to the stabilization of a magnetic leadscrew is considered. Resonance is shown to be completely eliminated. The stabilization time of the transient response is also significantly reduced, confirming the feasibility of the controller.**

***Index Terms*—Lightly damped systems, mode separation, neural network, passband control, regulation, stabilization, tuning regulator, vibration control.**

I. Introduction

MOST LIGHTLY damped structures are characterized by the presence of many elastic modes scattered over a wide frequency range. The dynamics of such structures may also be poorly known due to the difficulties in accounting for various damping effects and coupling gains. Depending on the applications, it may be desirable to suppress or sustain the oscillations. For example, the vibration suppression of flexible structures or lightly damped systems falls into the first category, whereas sensors, including the vibrating-beam accelerometers, require sustained oscillations to operate. Cancellation control such as command shaping ([3], [7], and [26]) and feedback Posicast [12] has been effective in reducing command-induced oscillations. However, such method does not suppress disturbance-induced vibrations or provide sustained oscillations. A number of learning controllers have been proposed for tracking periodic signals. In [19], an iterative feedforward-feedback learning controller is proposed for precision motion control of a permanent-magnet linear motor. In [20], single-neuron-based proportional-integral (PI) control is applied to vibration suppression. In [22] and [24], neural network is proposed for harmonic detection and damping of torsional vibrations. The use of fuzzy neural sliding-mode control for motion control is discussed in [21]. In [16], real-time implementation of neural-network controller is addressed. Observer-based vibration control has been proposed in [9] and [18]. Finally, the methods based on robust servomechanism and PI types of vibration control are given in [4], [14], and [27]. The conventional approach toward the stabilization and regulation of flexible structures typically consists of two steps: 1) modeling and 2) controller synthesis where, e.g., Kalman, filter-based stabilizers are designed. Whereas such methodology may be effective in dealing with lumped-parameter systems, the application to the control of flexible structures is generally inefficient, owing to the uncertain plant dynamics and the excessively high control bandwidth requirements. Controller design can be made more effective by recognizing that most lightly damped structures have energy content in a number of separate passbands, which are band limited. Each band can be considered to be a separate plant, and a modular structure can be obtained, as shown in Fig. 1, where the plant consists of N passband modules with outputs $Y_i(s)$.

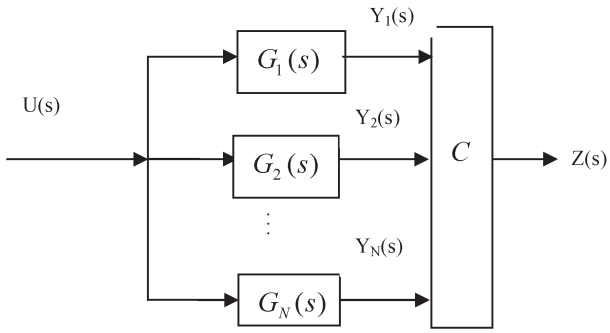

Fig. 1. Modular-plant structure.

However, the measured outputs $Z(s)$ are usually a linear combination of the passband outputs due to internal coupling and sensor placement. It is therefore necessary to extract the passband components from the measured output prior to carrying out feedback control. The band-limited nature of passbands suggests the use of the Hilbert transform which is known in the communication-system community for the key role it plays in the bandwidth conservation in single-sideband modulation. Because each oscillating mode can be treated as a separate narrowband modulation frequency centered around a carrier frequency, the Hilbert transform can then be used to obtain an equivalent model in the baseband for each of the individual modes of the plant (subsections of the controller).

In [2], a nonlinear tuning regulator (NTR) is devised to stabilize and regulate the elastic modes. Approximate knowledge of the resonant frequencies is required to operate the NTR. The bandpass nature of the resonant sections suggests the use

Manuscript received January 11, 2006; revised January 18, 2008.

The authors are with the Department of Electrical and Computer Engineering, New Jersey Institute of Technology, Newark, NJ 07102 USA (e-mail: changtn@njit.edu; ansari@njit.edu).

Color versions of one or more of the figures in this paper are available online at http://ieeexplore.ieee.org.

Digital Object Identifier 10.1109/TIE.2008.918610

of Hilbert transform [10] to translate the energy bands down to the baseband, where bandwidth-conservative control-system design can be carried out for each resonant section. The control action for each section is naturally decoupled from each other in the steady state due to the given frequency separation. Such decoupling gives rise to the modularity in the control system.

II. Plan Structure

The plant is assumed to be linear with the ith passband described by the following transfer function:

$$G_i(s) = \frac{H_i s}{s^2 + 2\zeta_i\omega_i s + \omega_i^2}, \qquad i = 1, 2, \ldots, N \tag{1}$$

where H_i is the high-frequency gain, and ζ_i and ω_i are the damping factor and the natural frequency of the ith mode, respectively. The individual passband outputs $Y_i(s)$ can be expressed as

$$Y_i(s) = G_i(s)U(s) \tag{2}$$

$$Y(s) = [Y_1(s), Y_2(s), \ldots, Y_N(s)]' \tag{3}$$

$$Z(s) = CY(s) \tag{4}$$

where $C \in \Re^{N\times N}$, and $Z(s)$ is the Laplace transform of the measured output $z(t) \in \Re^N$. In lightly damped systems, the natural frequency or, equivalently, the ringing frequency $\omega_i^d = \omega_i\sqrt{1-\zeta_i^2}$ or resonant frequency $\omega_i^r = \omega_i\sqrt{1-2\zeta_i^2}$ may be readily measured by either a frequency sweep or a white-noise excitation test. The quantities ζ_i and H_i are, however, usually uncertain, and they cannot be determined accurately. For the remainder of this paper, it is assumed that the lightly damped system is driven by a single actuator. The generalization to multi-input configuration can be made by using a similar approach. Because the open-loop system is lightly damped, the section outputs $y_i(t)$, $i = 1, 2, \ldots, N$ are therefore also narrowband given by

$$y_i(t) = A_i(t)\sin\left(\omega_i^d t + \theta_i(t)\right) \tag{5}$$

$$= y_i^c(t)\cos\omega_i^d t - y_i^s(t)\sin\omega_i^d t, \qquad i = 1, 2, \ldots, N \tag{6}$$

where $y_i^c(t)$ and $y_i^s(t) \in \Re$ are the baseband in-phase and quadrature components of $y_i(t)$, respectively. Let $\mathrm{amp}(y_i(t)) = \sqrt{(y_i^c)^2 + (y_i^c)^2}$ be defined as the amplitude of $y_i(t)$, and let y_i^{ref} be defined as the reference signal. $\mathrm{amp}(y_i(t))$ can be obtained from $y_i(t)$ by standard demodulation techniques.

Let the regulation error be defined as

$$e_i(t) = \mathrm{amp}\,(y_i(t)) - y_i^{\mathrm{ref}}, \qquad i = 1, 2, \ldots, N. \tag{7}$$

The control objectives [6] can then be expressed as follows.

1) Stabilization. $\mathrm{amp}(y_i(\infty)) = 0$, where $i = 1, 2, \ldots, N$;
2) Regulation. $e_i(\infty) = 0$, where $i = 1, 2, \ldots, N$;
3) Robustness. Properties 1) and 2) hold under small parametric perturbation in ζ_i, ω_i, and H_i, where $i = 1, 2, \ldots, N$.

Condition 2) mentioned earlier also implies 1) by setting y_i^{ref} to zero. In addition, it is desired to achieve the control objectives with minimal plant information. In this case, it is assumed that the number of lightly damped modes is known or can be measured.

III. Low-Frequency Equivalent Model

In this section, the low-frequency equivalence of $y_i(t)$ and the plant impulse response are derived via the Hilbert transform, following the approach of [10]. Denote $\mathfrak{H}(\bullet)$ as the Hilbert transform so that

$$\widehat{y}_i\,(t) = \mathfrak{H}\,[y_i(t)] \tag{8}$$

and define the pre-envelop of $y_i(t)$ as

$$\overline{y}_i(t) = y_i(t) + j\,\widehat{y}_i\,(t) \in C. \tag{9}$$

Then, it is observed that [10]

$$\begin{aligned} y_i(t) &= \mathrm{Re}\,[\overline{y}_i(t)] \\ &= \mathrm{Re}\left[\left(\overline{y}_i(t)e^{-j\omega_i^d t}\right)e^{j\omega_i^d t}\right] \\ &= \mathrm{Re}\left[\tilde{y}_i(t)e^{j\omega_i^d t}\right]. \end{aligned} \tag{10}$$

The quantity $\tilde{y}_i(t) = \overline{y}_i(t)e^{-j\omega_i^d t} \in C$ is known as the complex envelop of $y_i(t)$. $\tilde{y}_i(t)$ is a low-pass signal with bandwidth Ω_i, and it can be expressed as

$$\tilde{y}_i(t) = y_i^c(t) + jy_i^s(t) \tag{11}$$

where $y_i^c(t)$ and $y_i^s(t) \in \Re$ are the low-frequency in-phase and quadrature components of $y_i(t)$, respectively, as in (6). The section impulse-response matrix $G_i(t) = L^{-1}G_i(s)$ can also be decomposed into its low-frequency in-phase and quadrature pair $G_i^c(t)$ and $G_i^s(t)$ in a similar manner [10]

$$G_i(t) = 2G_i^c(t)\cos\omega_i^d t - 2G_i^s(t)\sin\omega_i^d t. \tag{12}$$

It is obvious that $G_i^c(t)$ and $G_i^s(t)$ are stable iff $G_i(t)$ is stable. The section output $y_i(t)$ can now be expressed as

$$y_i(t) = G_i(t) * u(t) = \mathrm{Re}\left[\overline{G}_i(t) * \overline{u}(t)\right] \tag{13}$$

where $\overline{G}_i(t) = G_i(t) + j\hat{G}_i(t)$, $\hat{G}_i(t) = \mathfrak{H}[G_i(t)]$, and "$*$" denotes convolution.

On letting

$$\tilde{y}_i(t) = \tilde{G}_i(t) * \tilde{u}(t) = (G_i^c(t) + jG_i^s(t)) * (u^c(t) + ju^s(t))$$

and observing that $y_i(t) = \mathrm{Re}[\tilde{y}_i(t)e^{j\omega_i^d t}]$, it follows that

$$y_i(t) = y_i^c(t)\cos\omega_i^d t - y_i^s(t)\sin\omega_i^d t \tag{14}$$

where

$$\begin{aligned} y_i^c(t) &= G_i^c(t) * u_i^c(t) - G_i^s(t) * u_i^s(t) \\ y_i^s(t) &= G_i^s(t) * u_i^c(t) + G_i^c(t) * u_i^s(t) \end{aligned}$$

$u_i^c(t)$ and $u_i^s(t)$ are the low-frequency components of $u(t)$ aligned in the ith passband. The baseband equivalent model of the ith section is now obtained as

$$Y_i^b(s) = G_i^b(s)U_i^b(s) \tag{15}$$

where

$$G_i^b(s) = \begin{bmatrix} G_i^c(s) & -G_i^s(s) \\ G_i^s(s) & G_i^c(s) \end{bmatrix} \tag{16}$$

and $Y_i^b = [Y_i^c \;\; Y_i^s]'$, and $U_i^b = [U_i^c \;\; U_i^s]'$. The plant output $y(t)$ is given as

$$y(t) = \begin{bmatrix} y_1^c(t)\cos\omega_1^d t - y_1^s(t)\sin\omega_1^d t \\ y_2^c(t)\cos\omega_2^d t - y_2^s(t)\sin\omega_2^d t \\ \vdots \\ y_N^c(t)\cos\omega_N^d t - y_N^s(t)\sin\omega_N^d t \end{bmatrix}$$
$$z(t) = Cy(t). \tag{17}$$

Furthermore, because the impulse response of $G_i(t)$ is given by

$$\frac{H_i}{\omega_i^d} e^{-\zeta_i\omega_i t}\left[-\zeta_i\omega_i \sin\omega_i^d t + \omega_i^d \cos\omega_i^d t\right] \tag{18}$$

$G_i^b(s)$ is then calculated as

$$G_i^b(s) = \frac{H_i}{2\omega_i^d(s+\zeta_i\omega_i)} \begin{bmatrix} \omega_i^d & \zeta_i\omega_i \\ -\zeta_i\omega_i & \omega_i^d \end{bmatrix}. \tag{19}$$

Hence, $G_i^b(s)$ has a lightly damped pole at $-\zeta_i\omega_i$. The stabilization of the plant requires the shift of all N poles further into the left-half plane. For lightly damped structures, $\zeta_i \approx 0$, and therefore, the transfer dynamics with respect to the controller becomes

$$\frac{H_i}{2(s+\zeta_i\omega_i)}, \qquad i = 1, 2, \ldots, N. \tag{20}$$

Now, because (20) is first order, a proportional control can readily stabilize the plant. A bandwidth-conservative controller can now be synthesized for each of the N resonant sections based on the low-frequency equivalent models (20) provided that the $y_i(t)$ components can be extracted.

IV. Neural Mode Separator (NMS)

The plant output $z(t) = Cy(t)$ is a mixture of the modes $y_i(t)$, where $i = 1, 2, \ldots, N$. Therefore, the proper separation of the y_i's must first be achieved before individual mode regulation can take place. It is possible that the mode separation can be carried out by utilizing bandpass filters which unavoidably increase the complexity of the loop dynamics. Furthermore, the use of dynamical filtering also requires the approximate knowledge of the mode frequencies: $\omega_1^r, \omega_2^r, \ldots, \omega_N^r$. For plants with varying operating conditions and, hence, frequencies, it is of general interest to replace the fixed bandpass filters by an intelligent front end such as neural network. The NMS used in this paper belongs to the class of recurrent neural network, i.e.,

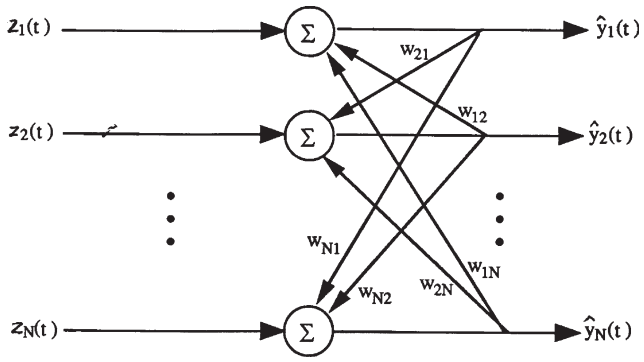

Fig. 2. NMS.

the outputs of the net are fed back to the input stage via a set of dynamic adaptive weights. NMS is a quasi-orthogonalization device. The objective is to blindly recover the modes from the mixture of modes. The term "blind" is used to signify the fact that the only information used to recover the modes is contained in the plant output $z(t)$. A general N-input–N-output NMS is shown in Fig. 2.

The following adaptation rules may be used to update the weights:

$$w_{ij}^+ = w_{ij}^- - \mu\alpha(\hat{y}_i)\beta(\hat{y}_j), \qquad i \neq j; \quad i, j \in [1, N]. \tag{21}$$

The parameter μ represents the learning rate, and $\alpha(\cdot)$ and $\beta(\cdot)$ are odd locally smooth functions. The origin of this scheme for a two-input–two-output system dates back to the '80s in the area of interference cancellation [1]. A justification of the mode separation for the case of elementary signals may be found in [17]. In this work, the elementary signals take on the form of resonant modes, and the statistical independence condition can be relaxed to the orthogonality between the modes

$$\langle y_i(t), y_j(t)\rangle = \lim_{T\to\infty} \frac{1}{2T} \int_{-T}^{T} y_i(t)y_j(t)\, dt = m_{ij}\delta_{ij} \tag{22}$$

where δ_{ij} is the Kronecker delta, and m_{ij} is a nonzero weight. Given that

$$\hat{y}(t) = (I - W)^{-1}z(t) = (I - W)^{-1}Cy(t)$$
$$C = [c_{ij}] = [\,\bar{c}_1 \quad \bar{c}_2 \quad \cdots \quad \bar{c}_N\,]$$

where

$$\bar{c}_i = \begin{bmatrix} c_{i1} \\ c_{i2} \\ \vdots \\ c_{iN} \end{bmatrix}, \qquad i = 1, 2, \ldots, N \tag{23}$$

$$W = \begin{bmatrix} 1 & w_{12} & w_{13} & \cdots & w_{1N} \\ & 1 & w_{23} & \cdots & w_{2N} \\ \vdots & & & \cdots & \vdots \\ w_{N1} & w_{N2} & w_{N3} & \cdots & 1 \end{bmatrix}. \tag{24}$$

In addition, let

$$(I-W)^{-1}=\begin{bmatrix}\psi_1\\ \psi_2\\ \vdots\\ \psi_N\end{bmatrix}$$

where ψ_i represents the ith row of $(I-W)^{-1}$, where $i=1,2,\ldots,N$

$$\begin{aligned}\langle\hat{y}_i(t),\hat{y}_j(t)\rangle &=\psi_i C\,\mathrm{diag}\left(\langle y_i(t),y_i(t)\rangle,\ i=1,\ldots,N\right)C'\psi_j'\\ &=\psi_i\left(\sum_{l=1}^{N}c_l c_l'\langle y_l(t),y_l(t)\rangle\right)\psi_j'\\ &=\psi_i\left(\sum_{l=1}^{N}c_l c_l' m_{ll}\right)\psi_j'. \end{aligned}\tag{25}$$

The objective of the weight adaptation is to minimize $\langle\hat{y}_i(t),\hat{y}_j(t)\rangle$, which attains a minimum if $\psi_i\bar{c}_j=0$, $i\neq j$, and $i,j=1,2,\ldots,N$ or, equivalently, if $(I-W)^{-1}C=P_N$ where P_N is a general permutation/scaling matrix. As the sections are structurally identical, P_N may be equated to the identity matrix I_N with no loss of generality. The degree of separation is thus determined by the value of $\langle\hat{y}_i(t),\hat{y}_j(t)\rangle$; the smaller this inner product, the higher is the degree of separation. Convergence characteristics and mode separation are illustrated in the numerical example given in Section VI. For the case of $N=2$

$$\begin{aligned}\left\langle\hat{y}_1^2\right\rangle&=\frac{(c_{11}+w_{12}c_{21})\left\langle y_1^2\right\rangle+(c_{12}+w_{12}c_{22})\left\langle y_2^2\right\rangle}{(1-w_{12}w_{21})^2}\\ \left\langle\hat{y}_2^2\right\rangle&=\frac{(c_{21}+w_{21}c_{11})\left\langle y_1^2\right\rangle+(c_{22}+w_{21}c_{12})\left\langle y_2^2\right\rangle}{(1-w_{12}w_{21})^2}\end{aligned}\tag{26}$$

with $\langle y_1,y_2\rangle=0$. The output power of the NMS is minimized if either

$$(w_{12},w_{21})\to\left(-\frac{c_{12}}{c_{22}},-\frac{c_{21}}{c_{11}}\right)\quad\text{or}\quad(w_{12},w_{21})\to\left(-\frac{c_{11}}{c_{21}},-\frac{c_{22}}{c_{12}}\right)$$

or equivalently

$$(I-W)^{-1}C\to\begin{bmatrix}m_{11}&0\\0&m_{22}\end{bmatrix}\qquad\text{or}\qquad\begin{bmatrix}m_{22}&0\\0&m_{11}\end{bmatrix}.$$

In the first case, $\hat{y}_1$ and $\hat{y}_2$ are directly proportional to y_1 and y_2, respectively, whereas in the second case, $\hat{y}_1$ and $\hat{y}_2$ are directly proportional to y_2 and y_1, respectively. Now, because $(\partial\langle\hat{y}_1^2\rangle/\partial w_{12})\propto\hat{y}_1\hat{y}_2$ and $(\partial\langle\hat{y}_2^2\rangle/\partial w_{21})\propto\hat{y}_1\hat{y}_2$, the following gradient-based updating rule may be used:

$$w_{ij}^{+}=w_{ij}^{-}-\mu\hat{y}_i\hat{y}_j,\qquad i\neq j;\quad i,j\in[1,2]\tag{27}$$

so that the adaptation ceases when $\hat{y}_i\to y_i$ and $\hat{y}_j\to y_j$, as the output power of the NMS becomes zero. This way, the NMS can be viewed as a quasi-orthogonalization device. The adaptation rule (21) is a more robust realization [17], and it is also the procedure used in this paper. Because the blind-source-separation problem, which has been widely studied and a variety of solutions have been proposed in the past decade, is not the main focus of this paper, readers are referred to [8], [11], [13], and [23] for further analyses and properties of the problem and solutions.

V. Controller Structure

The overall control objectives are the following: 1) closed-loop stability and 2) asymptotic regulation of the amplitude of each resonant mode of the flexible structure. Furthermore, it is desired to conserve control bandwidth so as to minimize implementation costs.

Because the dynamics of a flexible structure can be decomposed into N resonant subsystems whose energy is mainly distributed in the passband, the frequency-translation technique based on the Hilbert transform is first applied to the nominal plant to obtain a low-frequency equivalent model. Analysis and design are then carried out in the baseband to obtain the necessary bandwidth-conservative tuning regulator.

The neural-network front end is a single-layer recurrent net which separates the plant output back into the N frequency components (modes). The separated modes are then fed to the N structurally identical tuning-regulator modules. The tuning gains and the learning rate are derived by the online-tuning method. A set of N NTRs is synthesized to provide bandwidth conservative modular control of the N lightly damped sections. Each module has four components described as follows.

1) *Demodulator:* The conversion of $\hat{y}_i(t)$ into $\mathrm{amp}(y_i(t))$ may be achieved in various ways, e.g., envelop detection, synchronous demodulation, etc. For simplicity of description, envelope detection is chosen in this paper. The operation can be expressed as $(4/\pi)(|\hat{y}_i(t)|)$.
2) *Multiplier:* The function of the multiplier is to translate the controller output back to the original passband.
3) *Tuning gain ε_i:* The magnitude of this gain element is determined by online tuning to obtain satisfactory transient response. The polarity of ε_i is positive if the separated mode $\hat{y}_i$ is in phase with $y_i(t)$. Otherwise, it is taken to be negative.
4) *PI controller:* The stabilization and regulation of $\hat{y}_i(t)$ are effected by a PI controller having the form of $K(1+(K_I/s))$.
5) From (20), the equivalent baseband-characteristic equation for each mode is given by

$$s^2+(\varepsilon_i H_i/2+\zeta_i\omega_i)s+H_i K_I/2=0.\tag{28}$$

It is noted that the knowledge of the high-frequency gain H_i will be sufficient in choosing proper ε_i and K_I, so that the closed-loop poles are always in the left-half plane. With integral control in place, the asymptotic regulation and disturbance rejection for constant exogenous signals can be achieved [6]. For sinusoidal/periodic-disturbance rejection, the servocompensator approach may be applied [4].

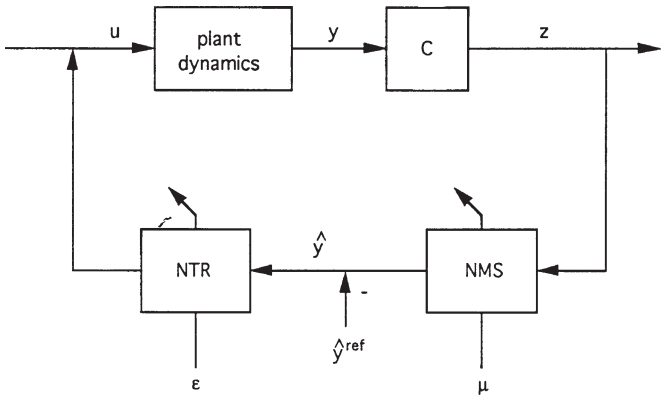

Fig. 3. Learning controller.

A block diagram showing the closed-loop control of a lightly damped structure is given in Fig. 3.

The following algorithm provides a systematic way of synthesizing the learning controller.

1) Determine the number of modes N (which is equal to the number of control modules).
2) Determine sensor location so that all N modes are observable.
3) Synthesize the NMS according to (3).
4) Synthesize the N NTR modules.
5) Adjust the learning rate μ so that satisfactory convergence is obtained.
6) Tune the system by adjusting ε_i online so that desirable transient characteristics are obtained. Reduce the magnitude of the integral gain if overshoot is excessive.

It is noted that for plant undergoing significant variations, retuning of μ and ε_i may be necessary to achieve better transient characteristics.

VI. Numerical Example

The aforementioned synthesis algorithm is now applied to the control of a lightly damped flexible structure with resonant frequencies at 300 and 400 rad/s. The nominal plant is described by the following equation:

$$\dot{x} = \begin{bmatrix} 0 & 1 & 0 & 0 \\ -300^2 & 0 & 0 & 0 \\ 0 & 0 & 0 & 1 \\ 0 & 0 & -400^2 & 0 \end{bmatrix} x + \begin{bmatrix} 0 \\ 1 \\ 0 \\ 1 \end{bmatrix} u$$

$$y = \begin{bmatrix} 0 & 1 & 0 & 2 \\ 0 & 2 & 0 & 1 \end{bmatrix} x.$$

The learning controller is tuned for the nominal plant, which subsequently is subjected to both (positive damping) stable and (negative damping) unstable perturbations. The controller parameters are as follows: $\mu = 0.000001$, $\varepsilon_1 = \varepsilon_2 = -15$, and $K_I = 4$.

These parameters are obtained by online tuning without the explicit knowledge of the plant. The input noise is applied for the first 2.5 s, whereas the NMS operates from 0 to 5 s.

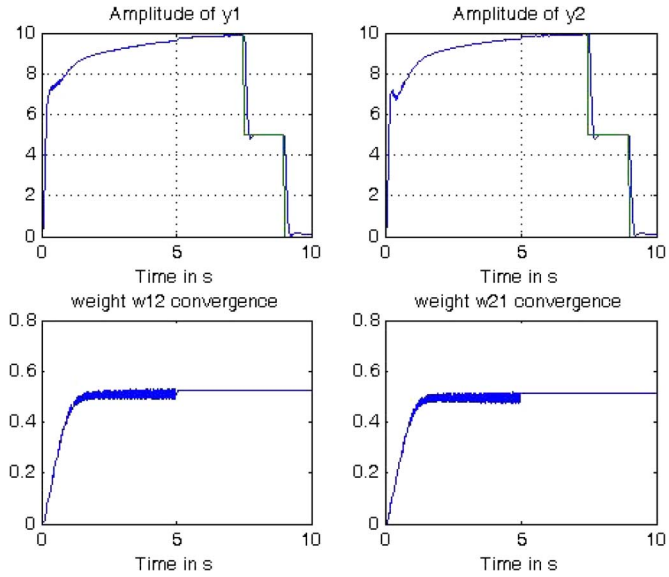

Fig. 4. Amplitude response of y_1, y_2, and weight adaptation.

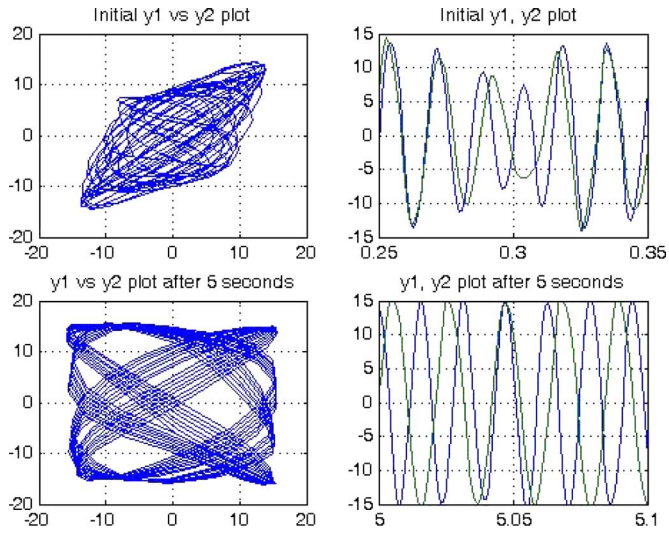

Fig. 5. Mode separation on y_1 and y_2.

The NTR operates continuously from 0 to 10 s, i.e., the entire simulation horizon.

The control profile is

$$\begin{aligned} y_1^{\text{ref}} = y_2^{\text{ref}} &= 10, \qquad t \in [0, 7.5] \\ &= 5, \qquad t \in [7.5, 9] \\ &= 0, \qquad t \in [9, 10]. \end{aligned}$$

The response of $\text{amp}(\hat{y}_i)$ is given in Fig. 4, along with the weight-convergence characteristics where it is observed that the convergence took place in about 1 s. The initial transient can be further modified by adjusting the controller gains. The asymptotic tracking of the control profile is observed. Fig. 5 shows the actual-mode response (upper trace) before and (lower trace) after weight convergence. The closeness of the mode frequencies is evident.

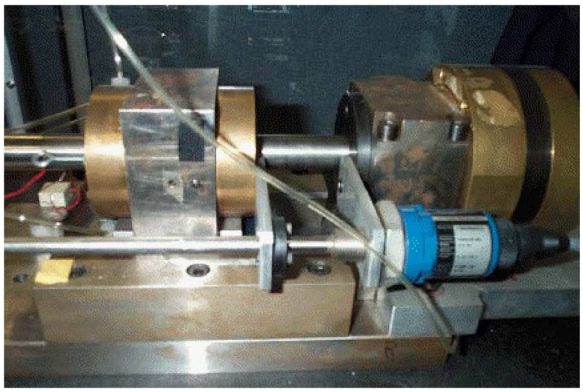

Fig. 6. Experimental setup of the magnetic leadscrew.

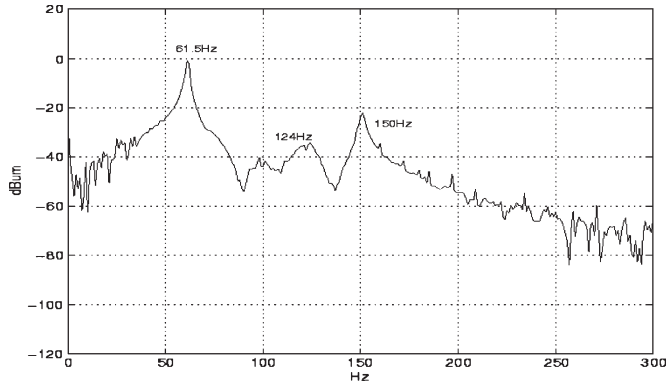

Fig. 7. Open-loop response of the plant.

VII. Application to a High-Precision Magnetic Leadscrew System

A magnetic leadscrew is a transmission device [5], [15], [25] by which rotary motion is converted into linear. A typical mechanical leadscrew transmission exhibits nonlinearities such as friction, backlash, and hysteresis, which limit the system performance significantly. The magnetic leadscrew in this example belongs to the class of contactless drives which overcome the aforementioned limitations of contact-type drives. The operation is based on leadscrew/nut coupling, but unlike mechanical leadscrews, the threads of the nut and the leadscrew are aligned magnetically and do not come in contact (see [15] for details of the modeling analysis). Thus, "hard" nonlinearities are substantially reduced, resulting in high precision and resolution. However, due to their contactless nature, magnetic leadscrews exhibit very low damping. The friction between transmitting parts is virtually eliminated, resulting in a lightly damped system which exhibits more vibration than conventional (contact-type) drives. This is an undesirable property inherent to these drives due to their contactless nature, and therefore, active-control schemes must be applied to suppress the vibrations. The experimental setup of the system is shown in Fig. 6.

The system consists of a nut and a leadscrew which are magnetically coupled to each other. The nut is mounted on a slide at the bottom and travels in the axial, i.e., the z-direction. The system uses lead zirconate–lead titanate (LZT-5) actuators to control the nut vibration. The controller is implemented on a PC-DSP development platform, which has a TMS320C31 floating point DSP. Two separate piezoelectric stacks with suitable proof mass are mounted on either side of the nut. One stack (piezoelectric transducer 1) is used to inject test disturbance, whereas the other (piezoelectric transducer 2) is used to produce the control motion. A low-G accelerometer and a capacitive sensor are mounted on the nut as shown to measure the axial (z-direction) acceleration and displacement of the nut, respectively. The capacitive sensor has a range of ± 25 μms which corresponds to the half rotation of the nut. The magnetic nut has an open-loop response, as shown in Fig. 7.

The conventional control of this system requires high-order high-sampling rate implementation. The design process is further complicated by the fact that the transfer function is load dependent, with uncertainty of the resonant frequencies. In the next section, the method of passband control is outlined. This method exploits the properties of resonant structures to produce a robust low order controller. The test procedure of the magnetic-leadscrew/nut-stabilization experiment consists of the following steps: First, the axial (z-direction) resonant modes are identified and characterized with respect to two loading conditions (1.1-and 2-kg load). Second, the NMS passband control is applied to stabilize these modes under two conditions: self-resonance and forced oscillation. For self-resonance, the nut is allowed to go into undamped oscillation (driven by background noise). The control objective here is to increase the damping, so that "ringing" is minimized. In the case of forced oscillation, a sinewave tuned to the resonant frequency is injected into the disturbance PZT, so that an oscillation is observed at the sensors. The goal is to reduce the transmission gain of the axial dynamics at the resonant frequencies. The test results for resonance suppression and transient improvements using the passband controller are now presented.

A. Resonance Suppression

The magnetic nut is subjected to considerable background noise and ground vibration, resulting in a pronounced "ringing effect" whenever additional mass is placed on top of the nut. The ringing is undesirable, considering the positioning demands on the drive. It is, however, observed that it has a single frequency of resonance and can therefore act as a candidate for external disturbance. The performance of the controller is evaluated in the presence of this self-resonance. From simulations, it was determined that $\mu = 10^{-11}$ was the most suitable value for an appreciable rate of learning and is the value for all tests conducted for both self-resonance as well as external disturbance.

1) $m = 1.1$-kg Load: A mass of 1.1 kg is added, and the effect of control is observed. Fig. 8 shows the (left) transient response of the nut, where the top graph is recorded with no control and the bottom graph shows the effects of the NMS-based control. Steady-state error is reduced from 0.91- to 0.026-μm root mean square (RMS). The fast Fourier transform (FFT) of the nut response also confirms that the self-resonance component is completely eliminated.

2) $m = 2$-kg Load: A second test run is conducted with an overall additional mass of 2 kg. The time response is shown

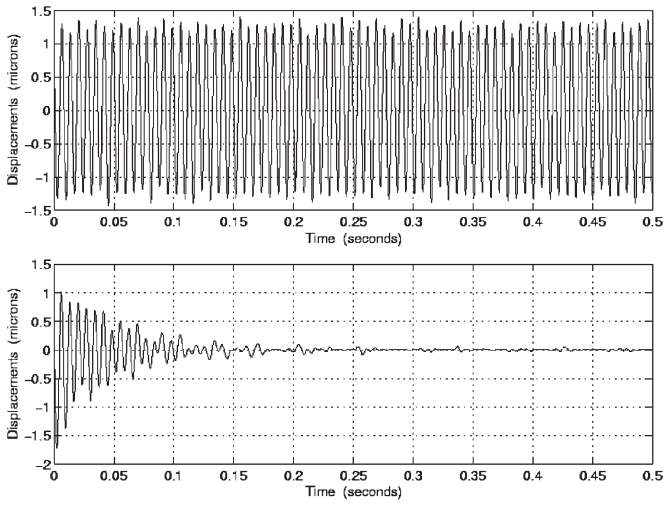

Fig. 8. Self-resonance cancellation: (top) no control and (bottom) with control.

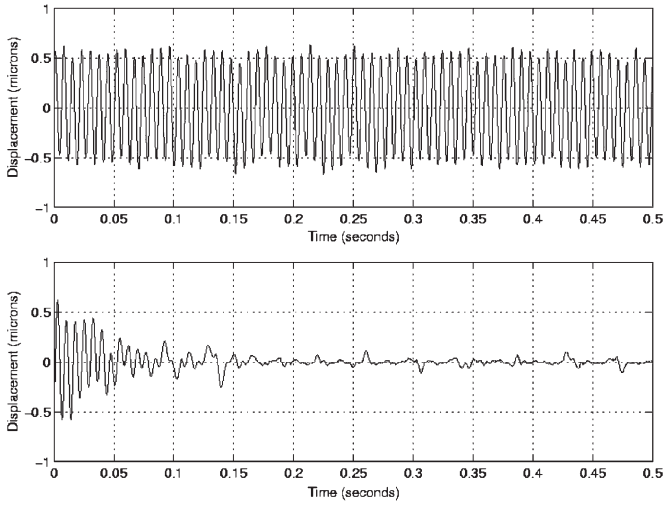

Fig. 9. Resonance suppression: (top) no control and (bottom) with control.

in Fig. 9 (top left: no control; bottom left: with control). The steady-state error is reduced from 0.40- to 0.023-μm RMS. Again, the FFT of the nut response confirms that the self-resonance component is eliminated.

B. Transient Improvement

This test is conducted to examine the improvement on transient response. An impulse input is applied by using a pendulum which makes an impact on the nut with the same impact force each time. Results are shown in Fig. 10.

It is observed that the time required for stabilization is significantly reduced under the control action. For this particular test configuration, the control is applied at mode one (61.5 Hz), which is the dominant mode of the nut, as shown in Fig. 7, and is the significant mode contributing to the vibration.

VIII. Conclusion

The control of lightly damped systems has been considered in this paper. Most lightly damped mechanical systems

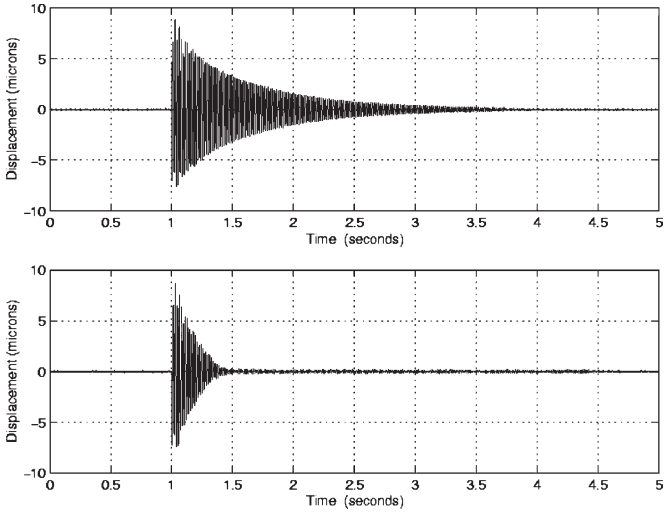

Fig. 10. Nut transient response: (top) no control and (bottom) with control.

exhibit significant parametric deviation and require accurate regulation by using a minimal-control bandwidth. The passband controller described in this paper combines a neural-network-based mode separator followed by a modular NTR. To carry out the controller design, it is only necessary to know the number of modes. Closed-loop response is then optimized online by adjusting a tuning gain for each modular section and the learning rate of the NMS. The combination of the NMS and NTR constitutes a special separation principle, where learning and regulation simultaneously take place. Finally, a numerical example with closely spaced mode frequencies and the experimental control of a magnetic leadscrew are considered to illustrate the feasibility and properties of this method.

References

[1] Y. Bar-Ness and J. Rokah, "Cross-coupled bootstrapped interference canceler," in *Proc. Int. Conf. Antennas Propag.*, Los Angeles, CA, Jun. 1981, pp. 292–295.
[2] T. N. Chang and N. Ansari, "A learning controller for the regulation and stabilization of flexible structures," in *Proc. IEEE Conf. Decision Control*, San Antonio, TX, Dec. 15–17, 1993, pp. 1268–1273.
[3] T. N. Chang, E. Hou, and K. Godbole, "Optimal input shaper design for high speed robotic workcells," *J. Vib. Control*, vol. 9, no. 12, pp. 1359–1376, Dec. 2003.
[4] T. N. Chang, R. Kwadzogah, and R. Caudill, "Vibration control of linear robots using piezoelectric actuator," *IEEE/ASME Trans. Mechatronics*, vol. 8, no. 4, pp. 439–445, Dec. 2003.
[5] T. N. Chang, B. Dani, Z. Ji, and R. Caudill, "Contactless magnetic transmission system: Vibration control and resonance compensation," *IEEE/ASME Trans. Mechatronics*, vol. 9, no. 2, pp. 458–461, Jun. 2004.
[6] T. N. Chang, "Servo control design," in *Encyclopedia of Life Support Systems*. New York: United Nations Educ., Sci., Cultural Org. (UNESCO), 2005.
[7] T. N. Chang, B. Cheng, and P. Sriwilaijaroen, "Motion control firmware for high-speed robotic systems," *IEEE Trans. Ind. Electron.*, vol. 53, no. 5, pp. 1713–1722, Oct. 2006.
[8] H. H. Dam, S. Nordholm, S. Y. Low, and A. Cantoni, "Blind signal separation using steepest descent method," *IEEE Trans. Signal Process.*, vol. 55, no. 8, pp. 4198–4207, Aug. 2007.
[9] A. Hace, K. Jezernik, and A. Sabanovic, "SMC with disturbance observer for a linear belt drive," *IEEE Trans. Ind. Electron.*, vol. 54, no. 6, pp. 3402–3412, Dec. 2007.
[10] S. Haykin, *Communication Systems*, 4th ed. Hoboken, NJ: Wiley, 2000.
[11] S. Haykin, *Neural Networks*, 2nd ed. Englewood Cliffs, NJ: Prentice-Hall, 1999.

[12] J. Y. Hung, "Feedback control with Posicast," *IEEE Trans. Ind. Electron.*, vol. 50, no. 1, pp. 94–99, Feb. 2003.
[13] A. Honkela, H. Valpola, A. Ilin, and J. Karhunen, "Blind separation of nonlinear mixtures by variational Bayesian learning," *Digit. Signal Process.: Rev. J.*, vol. 17, no. 5, pp. 914–934, Sep. 2007.
[14] K. Itoh, M. Iwasaki, and N. Matsui, "Optimal design of robust vibration suppression controller using genetic algorithms," *IEEE Trans. Ind. Electron.*, vol. 51, no. 5, pp. 947–953, Oct. 2004.
[15] Z. Ji, T. N. Chang, and R. Caudill, "Contactless magnetic leadscrew: Modeling and load determination," *IEEE Trans. Magn.*, vol. 36, no. 5, pp. 3824–3832, Sep. 2000.
[16] S. Jung and S. Kim, "Hardware implementation of a real-time neural network controller with a DSP and an FPGA for nonlinear systems," *IEEE Trans. Ind. Electron.*, vol. 54, no. 1, pp. 265–271, Feb. 2007.
[17] C. Jutten and J. Herault, "Blind separation of sources, Part I: An adaptive algorithm based on neuromimetic architecture," *Signal Process.*, vol. 24, no. 1, pp. 1–10, Jul. 1991.
[18] S. Katsura and K. Ohnishi, "Absolute stabilization of multimass resonant system by phase-lead compensator based on disturbance observer," *IEEE Trans. Ind. Electron.*, vol. 54, no. 6, pp. 3389–3396, Dec. 2007.
[19] T. H. Lee, K. K. Tan, S. Y. Lim, and H. F. Dou, "Iterative learning control of permanent magnet linear motor with relay automatic tuning," *Mechatronics*, vol. 10, no. 1/2, pp. 169–190, Feb. 2000.
[20] W. Li and Y. Hori, "Vibration suppression using single neuron-based PI fuzzy controller and fractional-order disturbance observer," *IEEE Trans. Ind. Electron.*, vol. 54, no. 1, pp. 117–126, Feb. 2007.
[21] F. J. Lin and P. H. Shen, "Robust fuzzy neural network sliding-mode control for two-axis motion control system," *IEEE Trans. Ind. Electron.*, vol. 53, no. 4, pp. 1209–1225, Aug. 2006.
[22] H. C. Lin, "Intelligent neural network-based fast power system harmonic detection," *IEEE Trans. Ind. Electron.*, vol. 54, no. 1, pp. 43–52, Feb. 2007.
[23] W. Liu, D. P. Mandic, and A. Cichocki, "Analysis and online realization of the CCA approach for blind source separation," *IEEE Trans. Neural Netw.*, vol. 18, no. 5, pp. 1505–1510, Sep. 2007.
[24] T. Orlowska-Kowalska and K. Szabat, "Neural-network application for mechanical variables estimation of a two-mass drive system," *IEEE Trans. Ind. Electron.*, vol. 54, no. 3, pp. 1352–1364, Jun. 2007.
[25] M. Shimanovich, R. Caudill, T. N. Chang, and Z. Ji, "Low friction high precision actuator," U.S. Patent 5 990 587, Nov. 23, 1999.
[26] N. Singer and W. Seering, "Preshaping command inputs to reduce system vibration," *Trans. ASME, J. Dyn. Syst., Meas. Control*, vol. 112, no. 1, pp. 76–82, Mar. 1990.
[27] K. Szabat and T. Orlowska-Kowalska, "Vibration suppression in a two-mass drive system using PI speed controller and additional feedbacks—Comparative study," *IEEE Trans. Ind. Electron.*, vol. 54, no. 2, pp. 1193–1206, Apr. 2007.

Timothy N. Chang (S'78–M'80) received the B.Eng. degree (with honors) from McGill University, Montreal, QC, Canada, in 1980, and the M.A.Sc. and Ph.D. degrees from the University of Toronto, Toronto, ON, Canada, in 1982 and 1989, respectively.

From 1987 to 1991, he was a Senior Research Specialist with the Kearfott Guidance and Navigation Corporation, NJ, where he was in charge of the Doppler mirror ring-laser-gyroscope program. He is a Professor and Coordinator of the Intelligent Systems Area, Department of Electrical and Computer Engineering, New Jersey Institute of Technology (NJIT), Newark. His research interests include real-time systems, high-precision systems, web-based decentralized control, and robotics. He is the holder of six U.S. patents with two patents pending.

Dr. Chang is a member of Sigma Xi and the American Society of Engineering Education, and he was a member of the Montville Township Board of Education from 2000 to 2003. He is also the Chairman of the North Jersey IEEE Control Systems Chapter and IEEE Student Branch Advisor at NJIT. He was a recipient of seven education awards at NJIT and was conferred the title of NJIT Master Teacher in 2003. He received the Thomas Edison Best Patent Award in 2007. His research has been supported by the National Science Foundation, National Institute of Justice, National Institute of Standards and Technology, Department of Transportation, N.J. Department of Higher Education, N.J. Commission on Science and Technology, and the U.S. Army Research and Development Engineering Center.

Nirwan Ansari (S'78–M'83–SM'94) received the B.S.E.E. degree (*summa cum laude*) from the New Jersey Institute of Technology (NJIT), Newark, in 1982, the M.S.E.E. degree from the University of Michigan, Ann Arbor, in 1983, and the Ph.D. degree from Purdue University, West Lafayette, IN, in 1988.

He was with the Department of Electrical and Computer Engineering, NJIT, as an Assistant Professor in 1988, where he has been a Full Professor since 1997. He has also assumed various administrative positions. He is the author of *Computational Intelligence for Optimization* (Springer, 1997; translated into Chinese in 2000) with E. S. H. Hou, and the Editor of *Neural Networks in Telecommunications* (Springer, 1994) with B. Yuhas. His current research focuses on various aspects of broadband networks and multimedia communications. He has also contributed over 100 refereed journal articles and numerous conference papers and book chapters. He also serves on the Editorial Boards of *Computer Communications*, the *Electronics and Telecommunications Research Institute Journal*, and the *Journal of Computing and Information Technology*.

Dr. Ansari initiated (as the General Chair) the First IEEE International Conference on Information Technology: Research and Education (ITRE2003), and was instrumental, while serving as its Chapter Chair, in rejuvenating the North Jersey Chapter of the IEEE Communications Society, which received the 1996 Chapter of the Year Award and the 2003 Chapter Achievement Award. He served as Chair of the IEEE North Jersey Section and on the IEEE Region 1 Board of Governors during 2001–2002. He has been serving on various IEEE committees such as Chair of the IEEE Communications Society Technical Committee on Ad Hoc and Sensor Networks, and (Technical Program Committee) Chair/Vice Chair of several conferences. He is a Senior Technical Editor of the *IEEE Communications Magazine*. He has been invited to deliver keynote addresses, distinguished lectures, tutorials, and talks at various conferences/workshops/symposia. His awards and recognition include the NJIT Excellence Teaching Award in Graduate Instruction (1998), IEEE Region 1 Award (1999), an IEEE Leadership Award (2007, from IEEE Princeton/Central Jersey Section), and designation as an IEEE Communications Society Distinguished Lecturer.